Observed Evidences of Frequency-Dependent Site Amplification Due to Structural Control of Active Reverse Faults at Different Localities in Japan

Mostafa Thabet (mostafa.thabet@aun.edu.eg)
Geology Department, Faculty of Science, Assiut University, Assiut 71516

Research Article

Keywords: Fault zone, Guided waves, Site response, Fourier spectrum, Spectral ratio, KiK-net and K-NET (Japan).

Posted Date: September 29th, 2021

DOI: https://doi.org/10.21203/rs.3.rs-606889/v2

Abstract

Observed active fault zone related site amplification is calculated based on Fourier acceleration spectrum (FAS) at three different localities in Japan. The FASs are calculated using 26432 earthquakes recorded at 126 K-NET and KiK-net seismic stations, which are distributed on the fault zones, upthrown and downthrown sides. This observed amplification is strongly frequency-dependent because of the presence of the near-surface low-velocity flower fault structure and the deeper fault zone. Moreover, the amplification patterns at each study area are tectonic-specific patterns. Sources inside the active fault zones could produce amplification at high frequencies at stations on both fault zone and far away from the fault zone, because of the impact of the near-surface fault zone. Sources outside the active fault zones yield remarkable high amplification at low frequencies exhibiting a gradual increase through stations on hanging walls, fault zones, and footwalls. Interestingly, the peaks of the low-frequency amplification are corresponding to wavelengths that approximately equalize the width of the fault zone. The presence of fault zone low-velocity layers could be successfully detected by the diffuse field theory inversion.

1. Introduction

Because many industrial and/or metropolitan areas are built on alluvial fans or basins, a correct quantification of the local site effects is necessary for a systematic and robust assessment of seismic hazards due to the direct relation with significant seismic damage and consequent loss of life. The amplification of an earthquake signal at a site plays a significant role in increasing seismic damage. The seismic site response due to fault zones has important implications on earthquake hazard on a local scale causing amplified motions near faults due to guided waves. Valuable research works by Li et al. (1994) on fault zone guided waves due to the San Andreas Fault zone grow attention to this issue. Constructive interference between reflected seismic waves is responsible for generating highly amplified fault zone guided waves and later arrivals of dispersive energy after *S*-waves (Igel et al. 1997). Fault gouge, clay-rich fault gouge, fracturing, increased porosity, remineralization, crack dilatation, and pore-fluid concentration near fault zones are the possible causes for this low-velocity zone (Ben-Zion 1998; Ben-Zion and Sammis 2003; Hickman et al. 2005).

Many researchers such as Rigano et al. (2008), Di Giulio et al. (2009), Pischiutta et al. (2012, 2013, 2015, 2017), Panzera et al. (2017a, 2017b), Burjánek et al. (2012), Panzera et al. (2019), Tortorici et al. (2019), and Kakhki et al. (2020) used the horizontal-to-vertical spectral ratios (HVSR) of earthquake and ambient vibration data to reveal the site effects related to fault zones. They observed systematic directional amplification normal to the dominant fault strike. Panzera et al. (2020) studied the site effects considering tectono-stratigraphic setting of the Santa Caterina area in Italy and observed maximum directional HVSR amplification of 8 in the perpendicular azimuth of the dominant N-S fracture zone. In contradict to these studies, Villani et al. (2018) did not observe any significant directional effects through their geophysical investigation at the Victoria fault in Malta. They interpreted their results because of the present inactivity in the fault zone, which is expressed in terms of ~ 0.6 Myr ago. Pischiutta et al. (2017)

found a predominant high horizontal amplification in the NE-SW to NNE-SSW direction (*i.e.* fault perpendicular direction) across the Vado di Corno fault in Italy, which is considered as active normal faults during the L'Aquila 2009 earthquake. Di Giulio et al. (2009) conducted dense microtremor measurements along and across the intensely fractured zones of the Pernicana fault, Mount Etna, Italy. They observed strong directional horizontal amplification at 1 Hz close to the highly fractured zone.

The existence of seismic stations across the fault provides a good opportunity in identifying these guided waves. According to studies by Igel et al. (2002), Jahnke et al. (2002), and Fohrmann et al. (2004), moderate variations of fault zone properties could produce guided waves. Seismogenic depths > 10 km could act as fault zone waveguide according to studies by Li et al. (1997, 2000, and 2004), Li and Vernon (2001), Korneev et al. (2003), Mizuno et al. (2004), and Mizuno and Nishigami (2006). Moreover, Ben-Zion (1998), Rovelli et al. (2002), Peng et al. (2003), and Lewis et al. (2005) proved significant trade-offs between propagation distance along the fault zone, fault zone width, impedance contrasts between massive and damaged rock, and source location. Fault zone-related site effects are extensively studied by many researchers in fault zone stations due to sources not necessarily in the fault zone. Li et al. (1990, 1997) used a small number of selected waveforms to study the fault zone guided waves due to 100 m wide of low-velocity fault zone extending to the seismogenic depth. In California, 1500 weak ground motions on fault zone arrays were studied by Li and Vernon (2001). Shallow fault zone could behave as a waveguide due to very deep ground motions and far from the fault zone (Jahnke et al. 2002; Igel et al. 2002; Fohrmann et al. 2004).

The role of active fault zones in affecting the earthquake hazard estimation is playing an important role in evaluating the seismic risk analyses. In Japan, a comprehensive database of active faults is provided by the National Institute of Advanced Industrial Science and Technology (AIST: https://gbank.gsj.jp/activefault/index_e_gmap.html, last accessed January 2021). These active faults are subdivided into several strands and characterized by their surface trace geometry, rupture history, slip per event, slip rate, calculated future rupture probability, and recurrence interval. These characteristics are evaluated based on paleoseismic and geologic studies. To improve the database system, all these characteristics are compiled based on previous studies, such as, Matsubara and Obara (2011), Nishida et al. (2008), Matsubara et al. (2008), Nakamura et al. (2008), Abdelwahed and Zhao (2007), Nakajima et al. (2001), Zhao et al. (1996), to cite few among many others. Therefore, the present research work is originated based on the AIST database of active faults in Japan.

Motivated by these valuable previous studies and the valuable AIST database of active faults, the present research work is established taking into account that strong variation in amplitude and frequency content of surface ground motions are strongly related to fault zone's geometry and seismic properties at depth. The present study is reported observed evidence of active reverse fault zone-related site spectral characteristics at three different localities in Japan using 26432 earthquakes recorded at 126 K-NET and KiK-net seismic stations. The spectral characteristics of the ground motions on the footwall (*i.e.* downthrown wall), fault zone, and the hanging wall (*i.e.* upthrown wall) are investigated by the Fourier acceleration spectrum of the surface orthogonal components, the HVSR, and the surface-to-borehole

spectral ratio. Comparisons among these techniques are also implemented as a procedure for identifying and analyzing site spectral amplifications. Considering that reverse faults at those three different localities in Japan have similar main fault strike, the resulted site spectral amplifications could be possibly inferred to the dominant fault dip, the dominant frequency caused by the fault zone width, and the different fracture patterns due to the existence of a dense network of minor and major active faults, and the seismic properties of the fault zone (*P*-wave and *S*-wave velocities, Poisson's ratio, and perturbation velocities).

2. Tectonic Patterns And Subsurface Tomography

In this study, active reverse faults with a predominant strike of north-south are studied. The study areas of this work (Fig. 1) are located in East Hokkaido, Akita-Iwate, and Fukushima in Japan.

The East Hokkaido active reverse faults, which are showing arc-shaped alignment, are composed of four major behavioral segments, including Shihoro, Otofuke, Tobetsugawa, and Kochien segments (Fig. 2). Table S1 is showing detailed characteristics of these behavioral segments as obtained from AIST (2013).

The active reverse fault system in the Akita-Iwate study area is composed of a set of several en-echelon behavioral segments (Fig. 3). Those behavioral segments of this active reverse fault system have their footwall blocks (*i.e.* downthrown sides) located on the right and left sides of the study area, whereas their hanging wall blocks (*i.e.* upthrown sides or the main fault zone) located in the center of the study area. As a result, the reverse fault system in the Akita-Iwate study area could be considered as a horst fault system. However, this active reverse fault system in the Akita-Iwate study area could be accommodated in three major parallel active reverse fault stands. Table S2 is summarizing the detailed characteristics of these behavioral segments as obtained from AIST (2013).

Fukushima's active fault system is composed of two sets of behavioral segments (Fig. 4). Table S3 is showing detailed characteristics of these behavioral segments as obtained from AIST (2013).

Understanding the physical properties of the subsurface structure of these large active reverse faults is an important step towards the understanding of the related site effects on those faults. AIST provides physical property in two-dimension subsurface structures, such as velocities of *P*-wave and *S*-wave, Poisson's ratio, and perturbation velocities of *P*-wave and *S*-wave, through their subsurface structures visualization system. In this research work, these physical property structures beneath the aforementioned active reverse faults are created and viewed for the profiles, which are selected beforehand in each study area. In the present paper, the velocities of *P*-wave and *S*-wave beneath the selected profiles are depending on the valuable study by Nakamura et al. (2008).

Figure 5 is showing *P*-wave and *S*-wave velocity structures along profile AB in the East Hokkaido study area (Figure S1 is showing detailed physical properties). The active reverse fault, which is dipping eastwards, extends to 30 km depth with Poisson's ratio of 2.2, and *P*-wave and *S*-wave velocities of 5.5 and 3 km/s, respectively. The intensely damaged and fractured fault material compared with the high

velocities of massive surrounding rocks (footwall and hanging wall blocks) are indicated by lower velocity perturbations of *P*-wave and *S*-wave (~ 8% lower than the initial velocity structures).

In the Akita-Iwate study area, CD and EF profiles are created and viewed using AIST's visualization system for subsurface structures based on Nakamura et al. (2008). The subsurface structures at CD and EF profiles are shown in Figure S2 and Figure S3, respectively. In profile CD, the reverse faults dipping eastwards, which are represented in reduced physical property, are seen particularly in the subsurface structures of *P*-wave velocity perturbations, whereas westwards dipping reverse faults are losing their reduced physical property evidence. Conversely, the reverse faults dipping westwards are seen in profile EF when compared with reverse faults dipping eastwards that are losing their reduced physical property evidence. This lateral discontinuity reveals that Akita-Iwate's fault system is undergoing a significant activity.

At profile GH in the Fukushima study area, the subsurface structures of *P*-wave and *S*-wave velocities, Poisson's ratio, and perturbation of *P*-wave and *S*-wave velocities are created and viewed in Figure S4 and Figure S5 based on Nakamura et al. (2008) and Nakajima et al. (2001), respectively. The reduced physical property in this active fault system could not be exhibited as seen in the East Hokkaido active fault system. This could be related to two reasons. First, the currently active fault trace could accommodate a maximum slip rate that is estimated at 0.1 m over about 1000 years with 2.4 m slip per event. Second, Fukushima active fault system might be young. Consequently, this lack of reduced physical properties has occurred clearly across the entire fault zone in the Fukushima study area.

3. Data

To study site spectral amplification across and along active reverse faults at the three different localities in Japan, K-NET and KiK-net database (https://www.kyoshin.bosai.go.jp, last accessed, January 2020) is used. Dense seismic stations of K-NET and KiK-net are present at those three different localities of the present study, which are the East Hokkaido, Akita-Iwate, and Fukushima study areas (Fig. 1).

Location maps of K-NET and KiK-net seismic stations in the East Hokkaido, Akita-Iwate, and Fukushima study areas are shown in Fig. 2, Fig. 3, and Fig. 4, respectively. Those stations located on the footwall (FW) block are differentiated from those located on the hanging wall (HW) block. Accordingly, earthquakes are also classified based on the locations of their hypocenters as earthquakes having their hypocenters beneath footwall (EFWs), fault zone (EFZs), and hanging wall (EHWs) blocks.

A total of manually selected 126 seismic stations, which are maintained by K-NET and KiK-net, are distributed on FW, FZ, and HW blocks at the three study areas. Additionally, a total of automatically selected 26432 earthquakes were recorded at those 126 K-NET and KiK-net seismic stations from May 1996 to January 2020. The selection of earthquakes depends on two criteria. First, only earthquakes with PGAs (*i.e.* Peak Ground Accelerations) of ≤ 10 cm/s^2 are used in the present study to characterize the linear response at each seismic station and avoid later modification due to nonlinear response (Thabet

2008, 2021a). Figure S6 is showing correlations between surface and borehole PGAs using KiK-net stations. Second, the hypocenters of these earthquakes must not exceed the predefined areas that are shown in Figs. 2, 3, and 4. Table 1 is summarizing the detailed numbers of seismic stations with their corresponding recorded earthquakes at the three study areas.

Ben-Zion et al. (2003) noted that stations located on the fault zone have motion amplification not only in the *S*-wave trains but also in the *P*-wave and other portions of the seismograms. Moreover, they observed that differences between waveforms recorded on fault zone and far from it are generated by nearly all events (*i.e.* on fault zone and far from it) and they exist not only in fault-parallel seismograms but also in the other components. Therefore, three orthogonal continuous time series are prepared at each seismic station in the present study based on the multiple-earthquakes approach of Thabet (2019, 2021b), which are representing EFWs, EFZs, and EHWs. Consequently, the structural control due to the presence of active reverse faults could be observed and interpreted at each seismic station. Figure S7 is showing an example of three continuous time series of east-west components (EW) at the TKCH05 KiK-net seismic station.

Table 1
Detailed numbers of seismic stations and recorded earthquakes at the three study areas.

		East Hokkaido		**Fukushima**			**Akita-Iwate**	
		K-NET	KiK-net	K-NET	KiK-net		K-NET	KiK-net
FW	Sta.	5	5	4	2	r.FW	16	11
	Eq.	2925		6618			6081	
FZ	Sta.	3	2	---	---	FZ	5	6
	Eq.	643		102		(Upthrown side)	3114	
HW	Sta.	17	10	14	8	l.FW	10	8
	Eq.	5806		570			573	

(Note: Sta. is station, Eq. is earthquake, FW is footwall block, FZ is fault zone, HW is hanging wall block, and r.FW and l.FW are right and left footwall blocks, respectively)

4. Methods

In engineering seismology, the site effects are usually studied in the frequency domain as variations of seismic wave's amplitude. There are various spectral ratio methods, which effectively reveal how active reverse fault zones modify the seismic waves. Since pioneering studies by Nogoshi and Igarashi (1970, 1971) and Nakamura (1989), horizontal-to-vertical spectral ratio is the usual technique for realistically estimate the predominant and fundamental frequencies at a site (Lermo and Chavez-Garcia 1993;

Seekins et al. 1996; Thabet 2019 and 2021b). The applicability of horizontal-to-vertical spectral ratio (HVSR) is tested by Rigano et al. (2008) concluding good results on the surface of faults.

Using Geopsy software (Wathelet 2005; http://www.geopsy.org), the Fourier acceleration spectrum (FAS) of the three orthogonal continuous time series and their HVSRs are calculated. During calculations, and following the SESAME (2004) guidelines, the reliability and quality of these FAS and HVSR calculations are checked to yield an acceptable level of scattering (*i.e.* acceptable low standard deviation values) that may significantly influence the physical meaning of the FAS and HVSR curves. At KiK-net seismic stations only, the surface-to-borehole spectral ratios SBSRs are calculated using the orthogonal FAS.

To estimate the site spectral amplification (SSA) at each seismic station, equations 1 through 4 are used.

$$SSA_{OH} = \frac{S_O}{S_H} SSA_{O/l.F} = \frac{S_O}{S_{l.F}} \quad (1)$$

$$SSA_{OF} = \frac{S_O}{S_F} SSA_{O/r.F} = \frac{S_O}{S_{r.F}} \quad (2)$$

$$SSA_{HF} = \frac{S_H}{S_F} SSA_{l.F/r.F} = \frac{S_{l.F}}{S_{r.F}} \quad (3)$$

$$SSA_{FH} = \frac{S_F}{S_H} SSA_{r.F/l.F} = \frac{S_{r.F}}{S_{l.F}} \quad (4)$$

where S could be FAS, HVSR, or SBSR curves (Note: left side equations are applied on the East Hokkaido and Fukushima study areas, whereas right side equations are applied on the Akita-Iwate study area). F, H, and O terms are referring to earthquakes located beneath footwall block, hanging wall block, and fault zone (*i.e.* hanging wall blocks in the Akita-Iwate study area), respectively. $r.F$ and $l.F$ terms are referring to earthquakes located beneath the right and left footwall blocks (Er.FWs and El.FWs), respectively, in the Akita-Iwate study area.
For the purpose of measuring how the active reverse faults modify the amplification spectrum, equations 3 and 4 are used at stations on FW in East Hokkaido and Fukushima study areas or right footwall (r.FW) block in Akita-Iwate study area, and HW in East Hokkaido and Fukushima study areas or left footwall (l.FW) block in Akita-Iwate study area, respectively. To quantify the behavior of the site spectral amplifications at seismic stations located on different fault blocks, the average site spectral amplifications are calculated and bounded with their minimum and maximum amplification.

To examine the velocity structures beneath the fault zones, earthquake HVSR (EHVSR) inversions are carried out using inversion code program developed by Nagashima et al. (2014), which is specifically designed for calculating the theoretical EHVSR based on the diffuse field concept. As a result, it would be possible to confirm the presence of the low-velocity fault zone.

5. Estimation Of Site Effects

The resulted site effects of the present analyses consist of (1) FASs of seismic stations located on FW, FZ, and HW blocks, independently, and (2) calculations of the averaged SSAs at each independent zone. In the following sections, results are presented with discussions to interpret the resulted amplification patterns at the three study areas in the present research work.

5.1 East Hokkaido Study Area

In the East Hokkaido study area, Figs. 12, 13, and 14 are showing FASs results for stations on FW, FZ, and HW blocks, respectively. Obviously, the recorded EFZs yield maximum Fourier amplitude in the high-frequency band (*i.e.* approximately > 3 Hz) at all stations (Fig. 6). Moreover, recorded EHWs yield maximum Fourier amplitude in the low-frequency band (*i.e.* approximately < 3 Hz), particularly at stations located on FW block and FZ (Figure S8 and Figure S9, respectively), whereas maximum FASs in the high-frequency band (*i.e.* approximately > 3 Hz) are observed at stations located on HW block (Figure S10). These frequency-dependent maximum Fourier amplitudes are strongly related to the presence of the active reverse fault system.

Figure 7 is an example of the generalized site spectral amplification patterns in the East Hokkaido study area that are independently exhibited for seismic stations on FW (Figure S11), FZ (Figure S12), and HW (Figure S13) blocks. The behaviors of SSA_{OH} and SSA_{OF} are showing overall similar amplification patterns. This consistency in amplification patterns is obviously exhibited in Figs. 15, 16, and 17 as a transition from high amplification at high frequencies to low amplification at low frequencies. This indicates that amplification due to earthquakes outside the fault zone (EFWs and EHWs) is larger than amplifications due to earthquakes inside the fault zone (EFZs) in the low-frequency band (the maximum amplifications at 0.5 Hz in the vertical components and 0.3 Hz in the EW and NS components). Conversely, at seismic stations located on FW and FZ, both behaviors of SSA_{HF} and SSA_{FH} are showing a transition from high amplification at low frequencies to low amplification at high frequencies. It is noteworthy that frequencies at transition points between high amplifications and low amplifications are 3 Hz, 2 Hz, and < 1 Hz at seismic stations on FW, FZ, and HW blocks, respectively. In this paper, these frequencies would be called pivoted frequencies (*i.e.* PF). The SSA_{FH} at seismic stations on the hanging wall is consistent without exhibiting PF. Table 2 is summarizing the highs and lows of the average of SSA_{OH}, SSA_{OF}, SSA_{HF}, and SSA_{FH} values considering the orthogonal components observed at FW, FZ, and HW blocks at the East Hokkaido study area. The high amplifications in the high-frequency bands (SSA_{OH} and SSA_{OF}) reveal the strong role of the deep FZ effects. The low amplification in the low-frequency (SSA_{OH} and SSA_{OF}) could be inferred to the strong role of the near-surface impedance effects of the FZ, which are obviously shown in $SSA_{HF}$and SSA_{FH}. The gradual increase of the low amplification through SSA_{OH}, SSA_{OF}, and SSA_{HF}(shown in Table 2) is reflecting the strong structural control of the HW compared with the weak role of the FW in amplifying the ground motions. For stations on the FW, the SSA_{OH} indicates that the effect of EFZs in the high-frequency is similar to the effect of EHWs in the low-frequency. However, it could be concluded from the amplification factors that the influence of sources inside the fault zone (EFZs) are higher than those outside the fault zone (EFWs and EHWs) in amplifying the ground motions.

Table 2
Summary of highs and lows of site spectral amplifications in the East Hokkaido study area deduced from Figs. 22, 23, and 24.

			SSA_{OH}	SSA_{OF}	SSA_{HF}	SSA_{FH}
Footwall	EW	H.	2.98	2.68	5.39	—
		L.	0.29	0.45	0.86	—
	NS	H.	3.15	3.15	4.05	—
		L.	0.35	0.57	0.89	—
	UD	H.	3.17	2.90	4.59	—
		L.	0.25	0.52	0.87	—
Fault zone	EW	H.	3.25	2.28	—	3.73
		L.	0.15	0.50	—	0.69
	NS	H.	3.35	2.39	—	3.53
		L.	0.18	0.49	—	0.65
	UD	H.	3.51	2.37	—	3.39
		L.	0.22	0.52	—	0.59
Hanging wall	EW	H.	3.14	2.46	—	1.61
		L.	0.69	0.74	—	1.10
	NS	H.	2.97	2.25	—	1.73
		L.	0.86	0.72	—	1.22
	UD	H.	2.98	2.66	—	1.77
		L.	0.71	0.71	—	1.09

Guided waves of fault zone could be produced due to earthquakes very close to or in the fault zone (Igel et al. 2002; Fohrmann et al., 2004; Li and Vidale, 1996; Jahnke et al., 2002). In the light of these studies, the FASs of the recorded EFZs favour the highest amplifications at stations on FW, FZ, and HW blocks in East Hokkaido study area (Figs. 12, 13, and 14). Their amplification patterns (SSA_{OH}, SSA_{OF}, SSA_{HF}, and SSA_{FH}) shown in Figs. 15, 16, and 17 are compatible with the recent study by Wu et al. (2008). They observed that earthquakes inside (*i.e.* EFZs) and outside (*i.e.* EFWs and EHWs) the fault zone could produce high amplification (*i.e.* guided waves) in the near-surface fault zone. This near-surface fault zone could guide waves at low-frequency, whereas the deep part of the fault zone could guide high-frequency waves (Wu et al., 2008). This frequency-dependent feature makes the guided waves

dominant in the earthquake seismogram after travelling far distances. The shallow layers of the fault system in the East Hokkaido study area resemble the top part of 'flower' structure (Figure S1). The significance of these shallow layers (*i.e.* low-frequency waveguide) for seismic shaking hazard is considerably higher than that associated with the deep fault zone layers (*i.e.* high-frequency waveguide), because of the ability to generate motion amplification from a much broader spatial distribution of earthquakes (*i.e.* EFZs, EFWs, and EHWs in the present study) as previously concluded by Seeber *et al.* 2000. This consideration is already mentioned and indicated as the amplification due to earthquakes outside the fault zone (EFWs and EHWs) are larger than amplifications due to earthquakes inside the fault zone (EFZs) in the low-frequency band (the maximum amplification at 0.5 Hz in the vertical components and 0.3 Hz in the EW and NS components). Additionally, the peculiar feature of the PF could be interpreted as the transition from PF of 3 Hz (at stations on FW correspond to high-frequency waveguide due to deep fault zone) through 2 Hz (at stations on FZ), and < 1 Hz (at stations on HW correspond to low-frequency waveguide due to shallow flower fault structure). The wavelengths matching or close to the width of the fault are corresponding to these dominant frequencies. Interestingly, the peaks of the low-frequency amplification of $SSA_{OH}$and SSA_{OF}, particularly for seismic stations on FZ, are corresponding to frequencies of 0.5 Hz (vertical components) and 0.3 Hz (EW and NS components). Moreover, the *P*-wave and *S*-wave velocities in the FZ are approximately 5 and 3 km/s, respectively (Figure S1). Consequently, the estimated wavelengths are 10 km that approximately equalize the FZ width in the East Hokkaido study area.

5.2 Akita-Iwate Study Area

In the Akita-Iwate study area, Figs. 18, 19, and 20 are showing the results of FASs for stations on l.FW, FZ (*i.e.* hanging wall blocks or upthrown sides), and r.FW blocks, respectively. The FASs of stations on l.FW and FZ, which are calculated using recorded earthquakes having their hypocenters beneath the right footwall block (Er.FWs), have the highest Fourier amplitudes in the low-frequency band (*i.e.* approximately < 5 Hz). Conversely, the highest Fourier amplitudes in the high-frequency band (*i.e.* approximately > 5 Hz) are prevailing in the FASs that are calculated using recorded earthquakes having their hypocenters beneath the left footwall block (El.FWs), as shown in Figure S14 and Figure S15. Seismic stations on the r.FW are exhibiting the highest Fourier amplitudes for FASs due to recorded El.FWs (Figure S16). Spectacular behavior of FASs, which are calculated using recorded EFZs, could be clearly seen in all seismic stations with approximately intermediate Fourier amplitudes, as generalized in Fig. 8.

Figure S17, Figure S18, and Figure S19 are exhibiting the site spectral amplification patterns in the Akita-Iwate study area for seismic stations on r.FW, FZ (*i.e.* hanging wall blocks), and l.FW blocks, respectively. The behavior of $SSA_{O/l.F}$ is remarkably variant.

Table 3 is summarizing the highs and lows of the averages of $SSA_{O/l.F}$, $SSA_{O/r.F}$, $SSA_{r.F/l.F}$, and $SSA_{l.F/r.F}$ values considering the orthogonal components observed at r.FW, FZ, and l.FW blocks at

Akita-Iwate study area. It could be concluded from the amplification factors that the influence of sources or earthquakes far away from the fault zone (El.FWs and Er.FWs) are higher than those in the fault zone (EFZs) in amplifying the ground motions.

5.3 Fukushima Study Area

Figure 9 is showing examples of the results of FASs in the Fukushima study area. Detailed results are exhibited in Figure S20 and Figure S21 for stations located on footwall and hanging wall blocks. Two observations are prevailing in this study area. First, FASs that are calculated using recorded EFZs have the highest Fourier amplitudes. Second, the amplitudes of FASs, which are calculated using recorded EHWs, are higher than those calculated using recorded EFWs.

Table 3
Summary of highs and lows of site spectral amplifications in the Akita-Iwate study area deduced from Figs. 25, 26, and 27.

			$SSA_{O/l.F}$	$SSA_{O/r.F}$	$SSA_{l.F/r.F}$	$SSA_{r.F/l.F}$
Right Footwall	EW	H.	0.90	2.02	8.85	—
		L.	0.29	0.94	2.66	—
	NS	H.	0.89	2.14	15.59	—
		L.	0.28	1.13	2.78	—
	UD	H.	1.08	2.12	9.05	—
		L.	0.30	1.03	2.45	—
Fault zone (Hanging wall blocks)	EW	H.	2.08	2.98	—	3.47
		L.	0.57	0.93	—	0.83
	NS	H.	1.83	3.28	—	3.59
		L.	0.56	0.91	—	0.69
	UD	H.	2.02	3.06	—	3.89
		L.	0.64	0.85	—	0.86
Left Footwall	EW	H.	9.37	2.54	—	15.63
		L.	0.50	0.30	—	0.24
	NS	H.	7.45	2.39	—	14.19
		L.	0.46	0.30	—	0.22
	UD	H.	8.29	2.91	—	14.96
		L.	0.49	0.30	—	0.25

Similar generalized site spectral amplification patterns in the Fukushima study area (Figure S22 and Figure S23) as previously seen in the East Hokkaido study area. At both FW and HW blocks, a transition from high amplification at high frequencies to low amplification at low frequencies is observed in the behaviors of SSA_{OH} and SSA_{OF}. The PFs are ~ 2 Hz and ~ 1 Hz at seismic stations located on FW and HW blocks, respectively. As previously discussed in the East Hokkaido and Akita-Iwate study areas, these high amplification in the high-frequency bands (> 2 Hz) reveal the strong role of the deep FZ effects, whereas the low amplification in the low-frequency bands (0.4 ~ 0.6 Hz) reveal the strong role of the near-surface impedance effects of the FZ. These low amplification factors are seen in both SSA_{OH} and SSA_{OF} indicates that the effect of EHWs and EFWs (sources outside the fault zone) is higher than the effect of the EFZs (sources inside the fault zone) in amplifying the ground motions.

Table 4 is summarizing the highs and lows of the averages of SSA_{OH}, SSA_{OF}, SSA_{HF}, and SSA_{FH} values considering the orthogonal components observed at FW and HW blocks at the Fukushima study area. Both high and low amplifications are reflecting the strong structural role of the HW in amplifying the ground motions at the expense of the FW block. This feature is similar to the study case in the East Hokkaido area. Moreover, the effect due to the recorded EHWs and EFWs is higher than those of the recorded EFZs in amplifying the ground motions at low frequencies and vice versa at high frequencies.

5.4 HVSR and SBSR

Figure S24 is showing examples of HVSRs at different K-NET and KiK-net seismic stations in the three present study areas. Figure S25 is showing examples of SBSRs at different KiK-net seismic stations. It is obvious that there are no significant responses that could be interpreted as the effect of strong structural control due to active reserve faults, which is contradicted to previous work by Rigano et al. (2008) who concluded good HVSR results on the surface of faults through testing the reliability of HVSR.

Table 4
Summary of highs and lows of site spectral amplifications in the Fukushima study area deduced from Figs. 28 and 29.

			SSA_{OH}	SSA_{OF}	SSA_{HF}	SSA_{FH}
Footwall	EW	H.	4.79	7.13	4.79	---
		L.	0.32	0.76	1.32	---
	NS	H.	6.14	7.24	4.40	---
		L.	0.26	0.44	1.07	---
	UD	H.	5.78	7.92	4.53	---
		L.	0.41	0.81	1.27	---
Hanging wall	EW	H.	2.72	7.91	---	2.11
		L.	0.59	1.07	---	0.45
	NS	H.	2.61	8.44	---	1.29
		L.	0.58	0.99	---	0.41
	UD	H.	3.02	8.70	---	1.89
		L.	0.58	0.68	---	0.41

5.5 EHVSR Inversion

In each study area, two seismic stations on each block (FW, FZ, and HW) are selected to run EHVSR inversion. However, the different three tectonic patterns in the present study are summarized in Figure S26 accompanying the resulted maximum averages of SSAs at high and low frequencies deduced from stations on each block.

Figure S27 is showing three examples of inverted EHVSR curves superimposed with their corresponding observed HVSR curves. Reasonable fitting between the observed and the inverted EHVSR curves could be achieved.

Reduced *P*-wave and *S*-wave velocity structures with respect to the surrounding fault blocks (*i.e.* FW, HW, r.FW, or l.FW) are concluded as inverted from stations on the fault zone system in the East Hokkaido study area (Fig. 10, Figure S28, and Figure S29).

6. Conclusion

This study has originated from the observation of systematic larger amplitudes of ground motion spectra at K-NET and KiK-net seismic stations at three different localities in Japan because of the presence of active faults (AIST, 2013). These active reverse fault zones could produce local amplification not only on these active faults but also far away from these faults (*i.e.* footwall and hanging wall blocks). Analyzing site response related to these fault zones using FAS is most effective than using HVSR or SBSR at the present study areas.

Comparable SSAs at seismic stations on fault zone and far away from the fault zone are resulted at high frequencies due to sources or earthquakes inside the active fault zones. At low frequencies, sources inside the active fault zones could favor higher SSAs at stations on FW and l.FW in Fukushima and Akita-Iwate study areas, respectively, than at stations on HW, FZ, and r.FW in both study areas. In the study area of East Hokkaido, observed amplification could not be produced due to sources inside the active fault zones at low frequencies. In East Hokkaido and Fukushima study areas, sources outside the fault zone could not produce significant SSAs at high frequencies, whereas remarkable high SSAs at low frequencies with a gradual increase from stations on HWs through FZs and FWs. The stations on r.FW and l.FW in Akita-Iwate study area exhibit similar SSAs due to sources outside the fault zone at low frequencies, whereas stations on the FZ (*i.e.* HWs) are exhibiting high SSAs at high frequencies.

The observed amplification patterns on FW, FZ, and HW are strongly related to the corresponding tectonic pattern (*i.e.* tectonic-specific pattern) and the frequency bands. The near-surface (*i.e.* low-velocity layers forming flower structure) fault zone could produce low-frequency amplification, whereas high-frequency amplification is inferred to the fault zone in depth. Interestingly, the peaks of the low-frequency amplification are corresponding to wavelengths approximately equalize fault zone's width, particularly in the East Hokkaido and Akita-Iwate study areas.

Using HVSR is not effective in the present study areas, which is contradicted to previous work by Rigano et al. (2008) who concluded good HVSR results on the surface of faults through testing the reliability of HVSR. Additionally, the observed horizontal components are showing comparable amplification patterns. This peculiar feature indicates the strong structural prevalence amplification due to active fault zone guided waves as exhibited in all motion components (horizontal and vertical).

Declarations

Acknowledgements

The author is highly appreciated and grateful to the National Research Institute for Earth Science and Disaster prevention (NIED) for making the valuable KiK-net and K-NET data available (DOI : 10.17598/NIED.0004). The author would appreciate and acknowledge providing the EHVSR inversion code by Prof. Fumiaki Nagashima (DPRI, Kyoto University). The author would appreciate and acknowledge the generous, valuable, and constructive comments and suggestions from the Editor and the reviewers.

Funding

The author states that this research work is not supported by any fund and no fund is received.

Conflicts of interest/Competing interests

The author states that there are not any conflicts of interests or competing interests

Availability of data and material

Any data in this research work would be available upon request immediately.

Code availability

Any software application or custom code in this research work would be available upon request immediately.

Authors' contributions

The submitting author confirm that he is a single author named in the manuscript is aware of the submission and has agreed for the paper to be submitted to *Scientific Reports*. I am acknowledging the consent requirements. I am very appreciated for your careful consideration.

References

1. Abdelwahed M F, Zhao D (2007) Deep structure of the Japan subduction zone. Phys. Earth Planet. Inter. 162: 32-52.
2. AIST (National Institute of Advanced Industrial Science and Technology, Active Fault Database of Japan), July 23, 2013 Version. Research Information Database DB095, National Institute of Advanced Industrial Science and Technology https://gbank.gsj.jp/activefault/index_e_gmap.html
3. Ben-Zion Y (1998) Properties of seismic fault zone waves and their utility for imaging low-velocity structure. *J. geophys. Res.* 103(12): 567–585.
4. Ben-Zion Y,Sammis C G (2003) Characterization of fault zones. *Pure appl. Geophys.* 160: 677–715.

5. Ben-Zion Y, Peng Z, Okaya D, Seeber L, Armbruster J G, Ozer N, Michael A J, Baris S, Aktar M (2003) A shallow fault-zone structure illuminated by trapped waves in the Karadere–Duzce branch of the North Anatolian Fault, western Turkey. *Geophys. J. Int.*152: 699–717.
6. Burjánek, J., Moore, J.R., Yugsi-Molina, F.X., Fäh, D., 2012. Instrumental evidence of normal mode rock slope vibration. Geophys. J. Int. 188 (2), 559–569. https://doi.org/10.1111/j.1365-246X.2011.05272.x.
7. Di Giulio, G., F. Cara, A. Rovelli, G. Lombardo, and R. Rigano (2009), Evidences for strong directional resonances in
intensely deformed zones of the Pernicana fault, Mount Etna, Italy, J. Geophys. Res., 114, B10308, doi:10.1029/2009JB006393
8. Fohrmann M, Igel H, Jahnke G, Ben-Zion Y (2004) Guided waves from sources outside faults: an indication for shallow fault zone structure?.*Pure Appl. Geophys.* 161: 2125–2137.
9. Hickman S H, Zoback M D, Ellsworth W L (2005) Structure and composition of the San Andreas Fault zone at Parkfield: Initial results from SAFOD Phase 1 and 2. *EOS, Trans. Am. geophys. Un.* 83(47): 237.
10. Igel H, Ben-Zion Y, Leary P (1997) Simulation of *SH* and *P-SV* wave propagation in fault zones. *Geophys. J. Int.* 128: 533–546.
11. Igel H, Jahnke G, Ben-Zion Y (2002) Numerical simulation of fault zone guided waves: accuracy and 3-D effects. *Pure Appl. Geophys.* 159: 2067–2083.
12. Jahnke G, Igel H, Ben-Zion Y (2002) Three-dimensional calculations of fault zone guided waves in various irregular structures. *Geophys. J. Int.* 151: 416–426.
13. Kakhki, M.K., Peters, F.C., Mansur, W.J., SadidKhoii, A., Rezaei, S., 2020. Deciphering site response directivity in landslide-prone slopes from ambient noise spectral analysis. Eng. Geol. 269, 105542 https://doi.org/10.1016/j.enggeo.2020.105542.
14. Korneev V A, Nadeau R M, McEvilly T V (2003) Seismological studies at Parkfield IX: fault-zone imaging using guided wave attenuation. *Bull. seism. Soc. Am.* 93: 1415–1426.
15. Lermo J, Chavez-Garcia FJ (1993) Site effect evaluation using spectral ratios with only one station. *Bull. seism. Soc. Am.* 83(5):1574–94.
16. Lewis M A, Peng Z, Ben-Zion Y, Vernon F L (2005) Shallow seismic trapping structure in the San Jacinto fault zone near Anza, California. *Geophys. J. Int.* 162: 867–881. doi:10.1111/j.1365-246X.2005. 02684.x.
17. Li Y G, Leary P C, Aki K, Malin P (1990) Seismic trapped modes in the Orville and San Andreas Fault zones. *Science* 249: 763–766.
18. Li Y G, Aki K, Adams D, Hasemi A, Lee W H K (1994) Seismic guided waves trapped in the fault zone of the Landers, California, earthquake of 1992. *J. geophys. Res.* 99: 11705–11722.
19. Li Y G, Ellsworth W L, Thurber C H, Malin P E, Aki K (1997) Fault zone guided waves from explosions in the San Andreas fault at Parkfield and Cienega Valley, California. *Bull. seism. Soc. Am.* 87: 210–221.

20. Li Y G, Vernon F L (2001) Characterization of the San Jacinto fault zone near Anza, California, by fault zone trapped waves. *J. geophys. Res.-Solid Earth* 106(30): 671–688.
21. Li Y G, Vidale J E, Aki K, Xu F (2000) Depth-dependent structure of the Landers fault zone from trapped waves generated by aftershocks. *J. geophys. Res.-Solid Earth* 105: 6237–6254.
22. Li Y G, Vidale J E (1996) Low-velocity fault-zone guided waves: numerical investigations of trapping efficiency. *Bull. seism. Soc. Am.* 86: 371–378.
23. Li Y G, Vidale J E, Cochran E S (2004) Low-velocity damaged structure of the San Andreas fault at Parkfield from fault zone trapped waves. *Geophys. Res. Lett.* 31: 2165, doi:10.1029/2001JB001456.
24. Matsubara M, Obara K, Kasahara K (2008) Three-dimensional P- and S-velocity structures beneath the Japan Islands obtained by high-density seismic stations by seismic tomography. Tectonophysics 454: 86-103. doi:10.1016/j.tecto.2008.04.016
25. Matsubara M, Obara K (2011) The 2011 Off the Pacific coast of Tohoku earthquake related to a strong velocity gradient with the Pacific plate. Earth Planets Space 63: 663-667. doi:10.5047/eps.2011.05.018.
26. Mizuno T, Nishigami K, Ito H, Kuwahara Y (2004) Deep structure of the Mozumi-Sukenobu fault, Central Japan, estimated from the subsurface array observation of fault zone trapped waves. *Geophys. J. Int.* 159: 622– 642.
27. Mizuno T, Nishigami K (2006) Deep structure of the Nojima Fault, southwest Japan, estimated from borehole observations of fault-zone trapped waves. *Tectonophysics* 417: 231–247.
28. Nagashima F, Matsushima S, Kawase H, Sánchez-Sesma FJ, Hayakawa T, Satoh T, Oshima M (2014) Application of horizontal-to-vertical (H/V) spectral ratios of earthquake ground motions to identify subsurface structures at and around the K-NET site in Tohoku, Japan. *Bull. seism. Soc. Am.* 104: 2288–2302. https://doi.org/10.1785/0120130219
29. Nakajima J, Matsuzawa T, Hasegawa A, Zhao D (2001) Three-dimensional structure of Vp, Vs, and Vp/Vs beneath northeastern Japan: Implications for arc magmatism and fluids. J. Geophys. Res. 106(21); 843-857.
30. Nakamura Y (1989) A method for dynamic characteristics estimations of subsurface using microtremors on the ground surface. Q Rep RTRI Jpn 30: 25–33.
31. Nakamura M, Yoshida Y, Zhao D, Takayama H, Obana K, Katao H, Kasahara J, Kanazawa T, Kodaira S, Sato T, Shiobara H, Shinohara M, Shimamura H, Takahashi N, Nakanishi A, Hino R, Murai Y, Mochizuki K (2008) Three-dimensional P- and S-wave velocity structures beneath Japan. Phys. Earth Planet. Inter. 168: 49-70.doi:10.1016/j.pepi.2008.04.017.
32. Nishida K, Kawakatsu H, Obara K (2008) Three-dimensional crustal S wave velocity structure in Japan using microseismic data recorded by Hi-net tiltmeters. J. Geophys. Res. 113: B10302. doi:10.1029/2007JB005395.
33. Nogoshi M, Igarashi T (1970) On the propagation characteristics estimations of subsurface using microtremors on the ground surface. J Seismol Soc Jpn 23: 264– 280.

34. Nogoshi M, Igarashi T (1971) On the amplitude characteristics of microtremor (Part 2). J SeismolSocJpn 24: 26–40.
35. Panzera, F., Halldorsson, B., Vogfjörð, K., 2017a. Directional effects of tectonic fractures on ground motion site amplification from earthquake and ambient noise data: a case study in South Iceland. Soil Dyn. Earthq. Eng. 97, 143–154. https://doi.org/10.1016/j.soildyn.2017.03.024.
36. Panzera, F., Lombardo, G., Longo, E., Langer, H., Branca, S., Azzaro, R., Cicala, V., Trimarchi, F., 2017b. Exploratory seismic site response surveys in a complex geologic area: a case study from Mt. Etna volcano (southern Italy). Nat. Hazards 86, 385–399. https://doi.org/10.1007/s11069-016-2517-4.
37. Panzera, F., D'Amico, S., Colica, E., Viccaro, M., 2019. Ambient vibration measurements to support morphometric analysis of a pyroclastic cone. Bull. Volcanol. 81 (12), 74. https://doi.org/10.1007/s00445-019-1338-1.
38. Panzera F, Tortorici G, Romagnoli G, Marletta G, Catalano S (2020) Empirical evidence of orthogonal relationship between directional site effects and fracture azimuths in an active fault zone: The case of the Mt. Etna lower eastern flank. Engineering Geology 279 (2020) 105900, https://doi.org/10.1016/j.enggeo.2020.105900
39. Peng Z, Ben-Zion Y, Zhu L, Michael A J (2003) Inference of a shallow fault zone layer in the rupture zone of the 1992. Landers, California earthquake fro locations of events generating trapped waves and travel time analysis. *Geophys. J. Int.* 155: 1021–1041.
40. Pischiutta, M., Salvini, F., Fletcher, J.B., Rovelli, A., Ben-Zion, Y., 2012. Horizontal polarization of ground motion in the Hayward fault zone at Fremont, California: dominant fault-high-angle polarization and fault-induced cracks. Geophys. J. Int. 188 (3), 1255–1272. https://doi.org/10.1111/j.1365-246X.2011.05319.x.
41. Pischiutta, M., Rovelli, A., Salvini, F., Di Giulio, G., Ben-Zion, Y., 2013. Directional resonance variations across the Pernicana fault, Mt. Etna, in relation to brittle deformation fields. Geophys. J. Int. 193 (2), 986–996. https://doi.org/10.1093/gji/ggt031.
42. Pischiutta M, Savage M K, Holt R A, Salvini F (2015) Fracture-related wavefield polarization and seismic anisotropy across the Greendale Fault. J. Geophys. Res. Solid Earth 120: 7048–7067. doi:10.1002/2014JB011560.
43. Pischiutta, M., Fondriest, M., Demurtas, M., Magnoni, F., Di Toro, G., Rovelli, A., 2017. Structural control on the directional amplification of seismic noise (Campo Imperatore, Central Italy). Earth Planet. Sci. Lett. 471, 10–18. https://doi.org/10.1016/j.epsl.2017.04.017.
44. Rigano R, Cara F, Lombardo G, Rovelli A (2008) Evidence of ground motion polarization on fault zones of Mount Etna volcano. J Geophys Res. 113: B10306. http://dx.doi.org/10.1029/2007JB005574.
45. Rovelli A, Caserta A, Marra F, Ruggiero V (2002) Can seismic waves be trapped inside an inactive fault zone? The case study of Nocera Umbra, central Italy. *Bull. seism. Soc. Am.* 92: 2217–2232.
46. Seeber L, Armbruster J G, Ozer N, Aktar M, Baris S, Okaya D, Ben-Zion Y, Field E (2000) The 1999 Earthquake Sequence along the North Anatolia Transform at the Juncture between the Two Main

Ruptures, in The 1999 Izmit &Duzce Earthquakes: preliminary results. edit. Barka A., O. Kazaci, S. Akyuz& E. Altunel, Istanbul technical university, 209-223.

47. Seekins LC, Wennerberg L, Marghereti L, Liu HP (1996) Site amplification at five locations in San Fransico, California: a comparison of S waves, codas, and microtremors. *Bull. seism. Soc. Am.* 86(3): 627–35.
48. SESAME (2004) Guidelines for the implementation of the H/V spectral ratio technique on ambient vibrations: Measurements, processing and interpretation, SESAME (Site Effects Assessment Using Ambient Excitations. EC-RGD, Project No. EVG1-CT-2000-00026 SESAME), European Research Project WP12, deliverable D23.12, at http://sesame-fp5.obs.ujfgrenoble.fr/Deliverables 2004
49. Thabet M, Nemoto H, Nakagawa K (2008) Variation process in stiffness inferred by nonlinear inversion during mainshocks at Kushiro Port vertical array site. *Earth Planet Sp* 60: 581–589. https://doi.org/10.1186/BF03353121
50. Thabet M (2019) Site-Specific Relationships between Bedrock Depth and HVSR Fundamental Resonance Frequency Using KiK-NET Data from Japan. *Pure Appl. Geophys.* 176: 4809–4831. https://doi.org/10.1007/s00024-019-02256-7
51. Thabet M (2021a) Nonlinearity evaluation considering the uncertainty of *S*-wave velocity based on total stress analyses and diffuse field assumption: the M_w 9.1 great Tohoku Taiheiyo-Oki earthquake at 05:46 UTC on 11 March 2011. *J Seismol*. https://doi.org/10.1007/s10950-020-09974-9
52. Thabet M (2021b) Improved site-dependent statistical relationships of VS and resonant frequency versus bedrock depth in Japan. *J Seismol*. https://doi.org/10.1007/s10950-021-10038-9
53. Villani, F., D'Amico, S., Panzera, F., Vassallo, M., Bozionelos, G., Farrugia, D., Galea, P., 2018. Shallow high-resolution geophysical investigation along the western segment of the Victoria Lines Fault (island of Malta). Tectonophysics 724–725, 220–233. https://doi.org/10.1016/j.tecto.2018.01.010.
54. Tortorici, G., Romagnoli, G., Grassi, S., Imposa, S., Lombardo, G., Panzera, F., Catalano, S., 2019. Quaternary negative tectonic inversion along the Sibillini Mts. Thrust zone: the Arquata del Tronto case history (Central Italy). Environ. Earth Sci. 78 (1), 37. https://doi.org/10.1007/s12665-018-8021-2.
55. Wathelet M (2005) Array Recordings of Ambient Vibrations: Surface-Wave Inversion. Ph.D. thesis, Liège University, Belgium.
56. Wu J, Hole J A, Snoke J A, Imhof M G (2008) Depth extent of the fault-zone seismic waveguide: effects of increasing velocity with depth. *Geophys. J. Int.* 173: 611–622. doi: 10.1111/j.1365-246X.2008.03755.x
57. Zhao D, Kanamori H, Negishi H, Wiens D (1996) Tomography of the source area of the 1995 Kobe earthquake: Evidence for fluids at the hypocenter?. Science 274: 1891-1894.

Figures

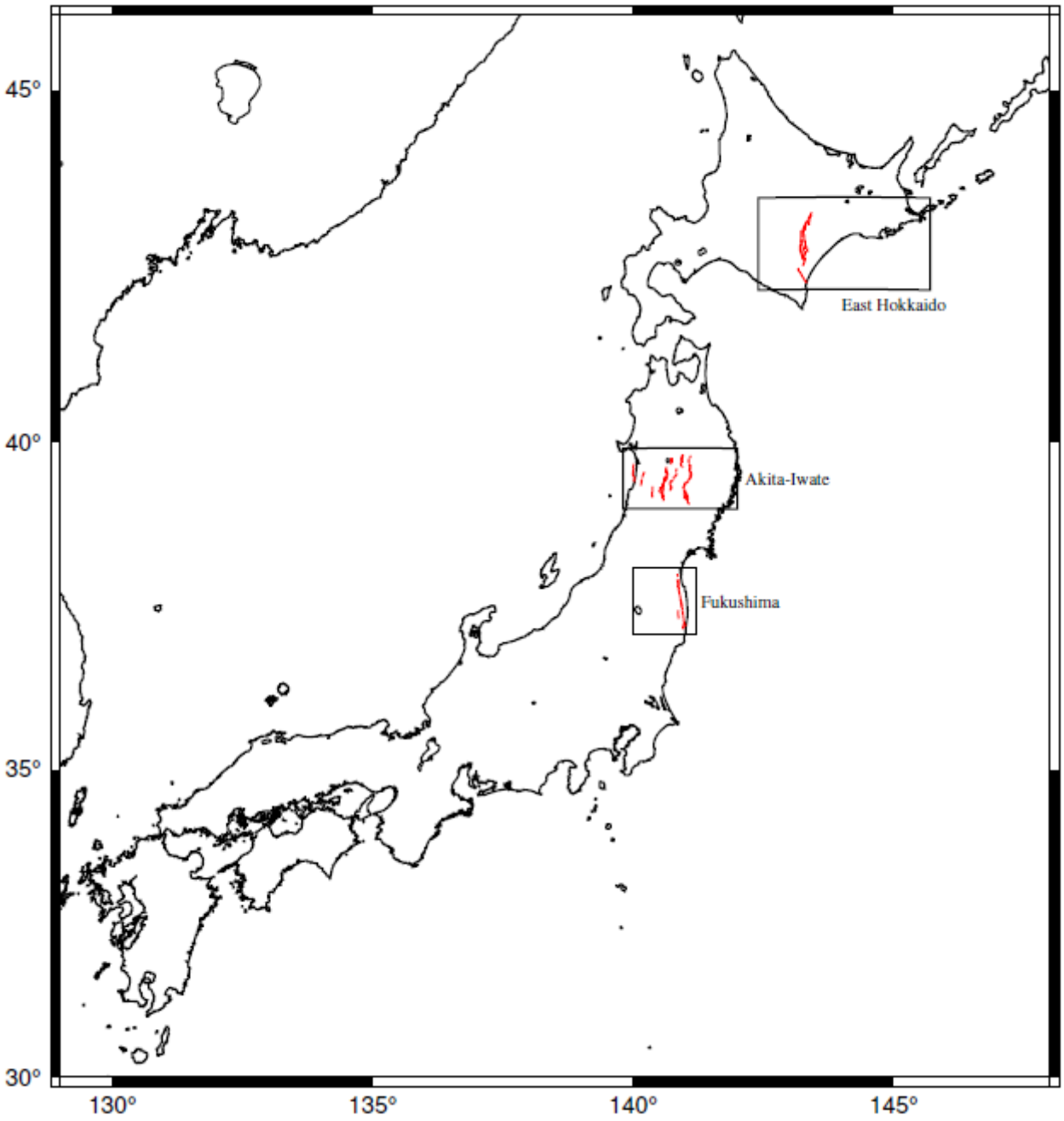

Figure 1

Location map for the three different study areas of East Hokkaido, AkitaIwate, and Fukushima in Japan that are used in the present study. (Note: red lines are representing the active reverse fault traces)

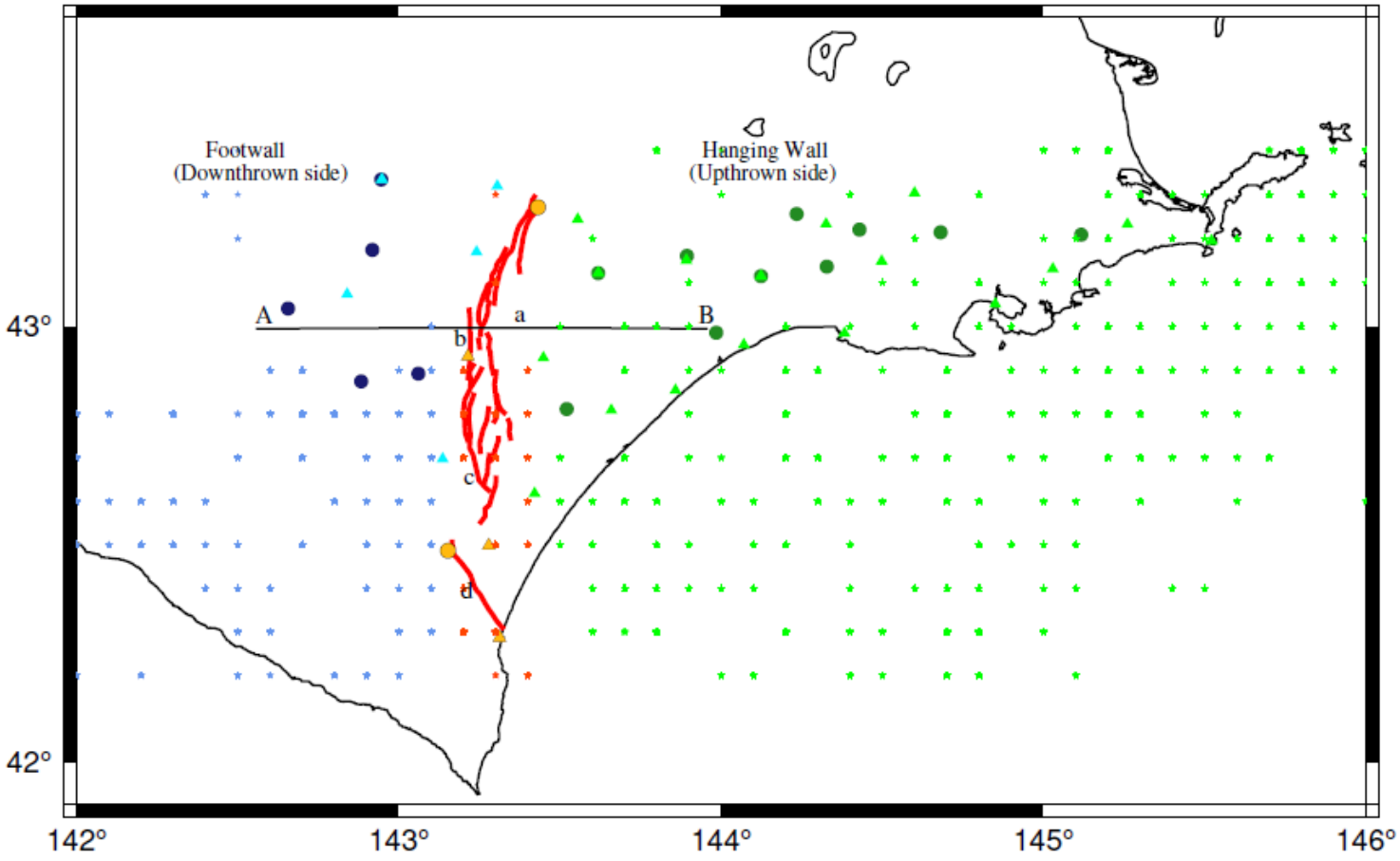

Figure 2

Distribution of KNET (triangles) and KiKnet (circles) seismic stations and the recorded earthquakes in East Hokkaido study area. (Note: On map, the colors of blue, yellow/red, and green are used to discriminate seismic stations/earthquakes located on and beneath FW, FZ, or HW, respectively. Red lines on map are representing active reverse fault traces. AB is profile across fault zones.)

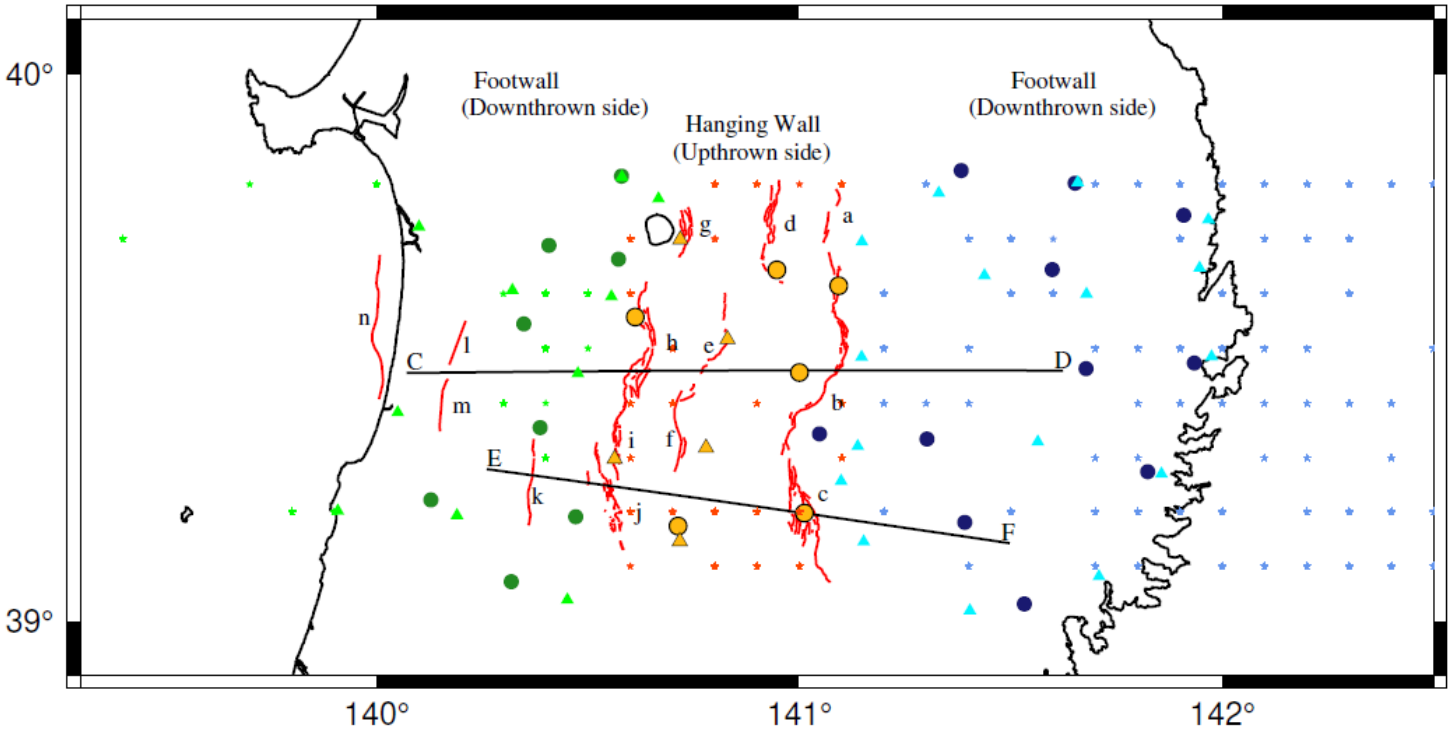

Figure 3

Distribution of KNET (triangles) and KiKnet (circles) seismic stations and the recorded earthquakes in Akitalwate study area. (Note: On map, the colors of green, blue, and yellow/red are used to discriminate seismic stations/earthquakes located on left and right footwall blocks, and fault zone, respectively. Red lines on map are representing active reverse fault traces. CD and EF are profiles across fault zones.)

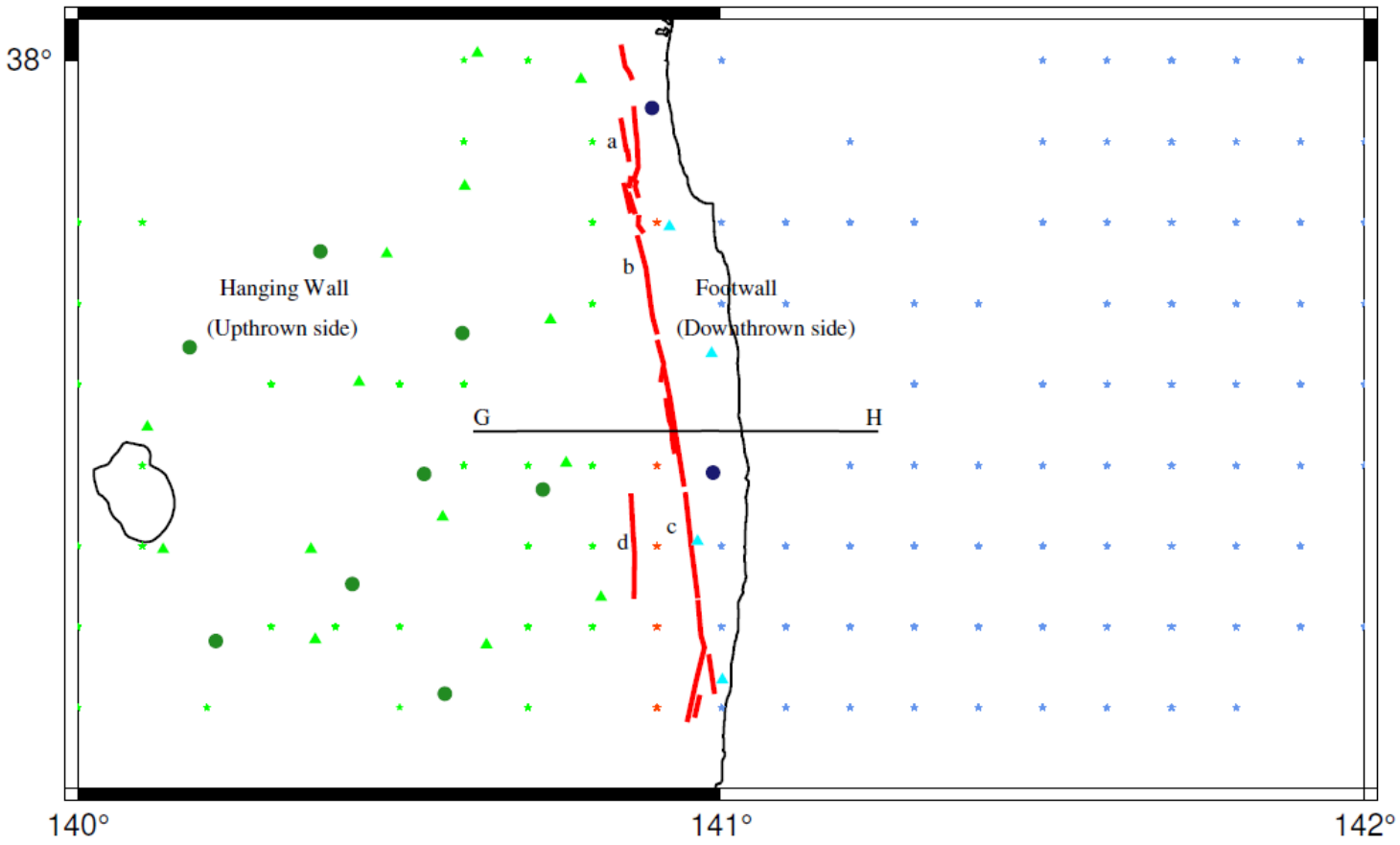

Figure 4

Distribution of K-NET (triangles) and KiK-net (circles) seismic stations and the recorded earthquakes in Fukushima study area. (Note: On map, the colors of green, red, and blue are used to discriminate seismic stations/earthquakes located on HW, FZ, and FW, respectively. Red lines on map are representing active reverse fault traces. GH is profile across fault zones.)

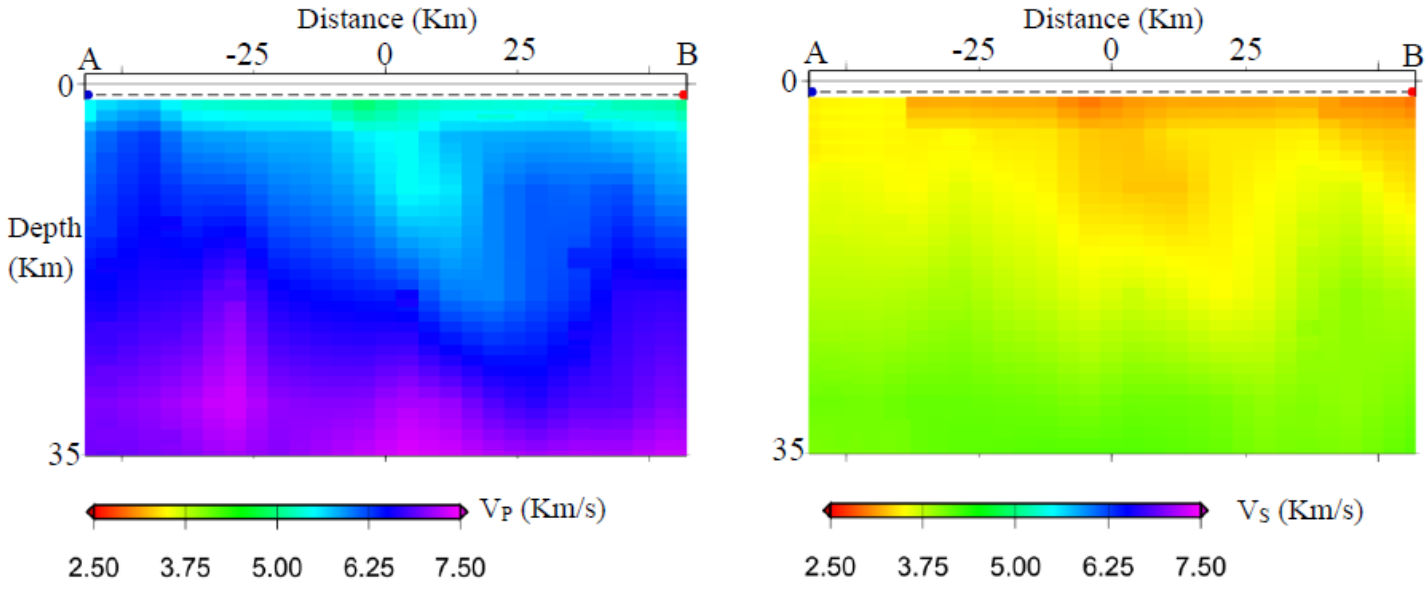

Figure 5

An example subsurface tomography structures along profile AB in East Hokkaido study area.

Figure 6

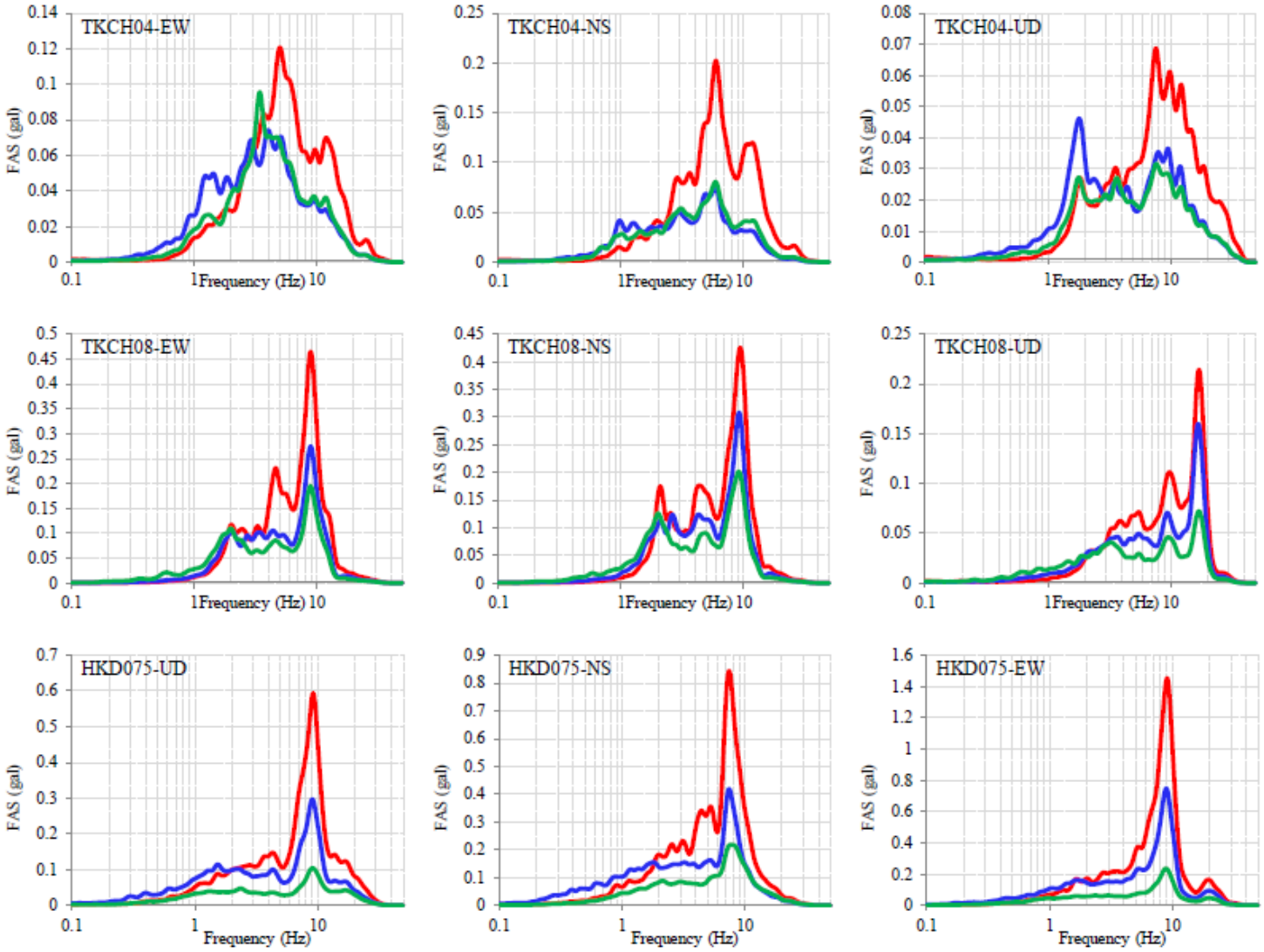

Examples of FASs at seismic stations located on FW (upper), FZ (middle), and HW (lower) blocks in the East Hokkaido study area due to recorded EFWs (blue), EFZs (red), and EHWs (green).

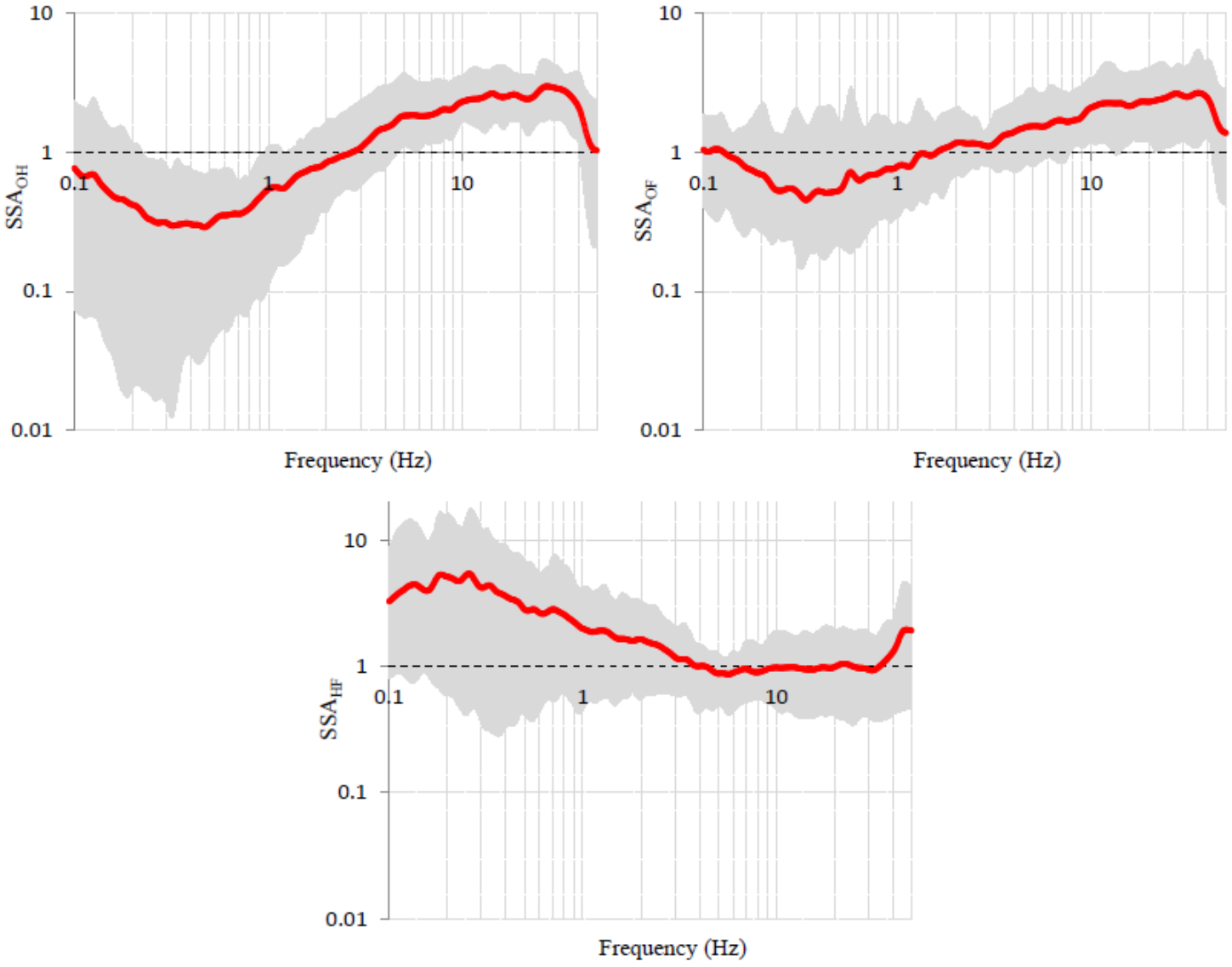

Figure 7

An example of the estimated average SSAs (red) of EW component with their minimum and maximum (gray), which are calculated based on equations 1, 2, and 3 for the seismic stations located on the FW block in East Hokkaido study area.

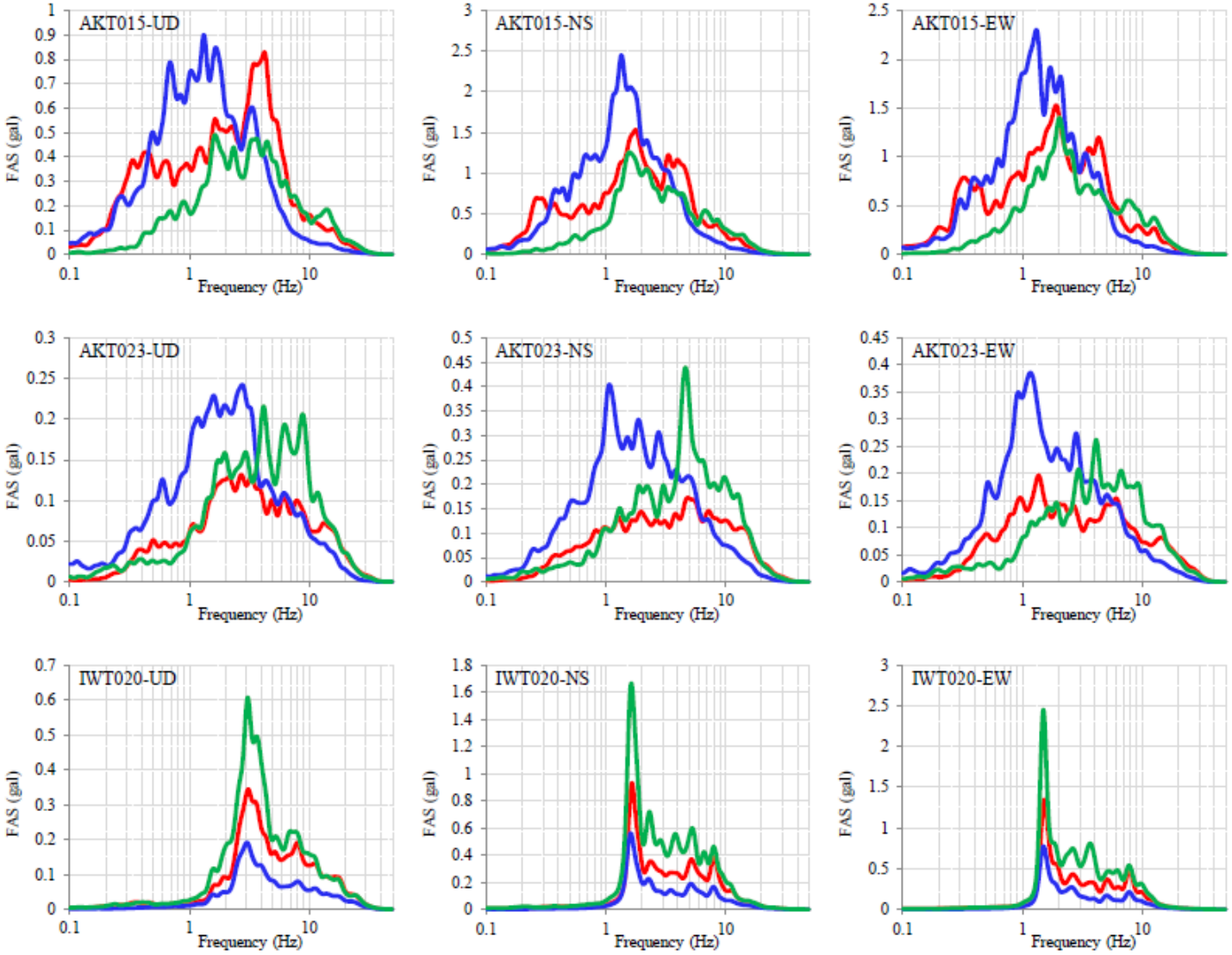

Figure 8

Examples of FASs at seismic stations located on l.FW (upper), FZ (middle), and r.FW (lower) blocks in Akita-Iwate study area due to recorded El.FWs (green), EFZs (red), and Er.FWs (blue).

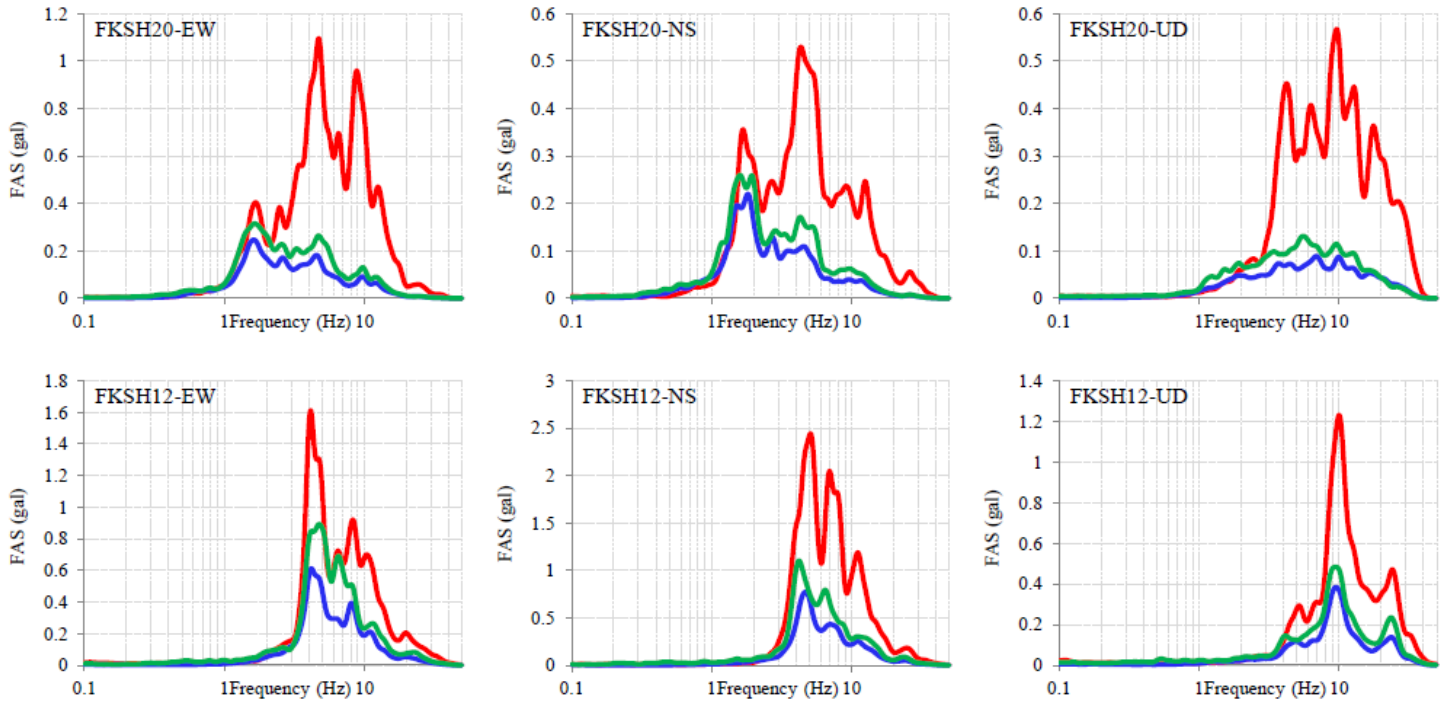

Figure 9

Examples of FASs at seismic stations located on FW (upper) and HW (lower) blocks in Fukushima study area due to recorded EFWs (blue), EFZs (red), and EHWs (green).

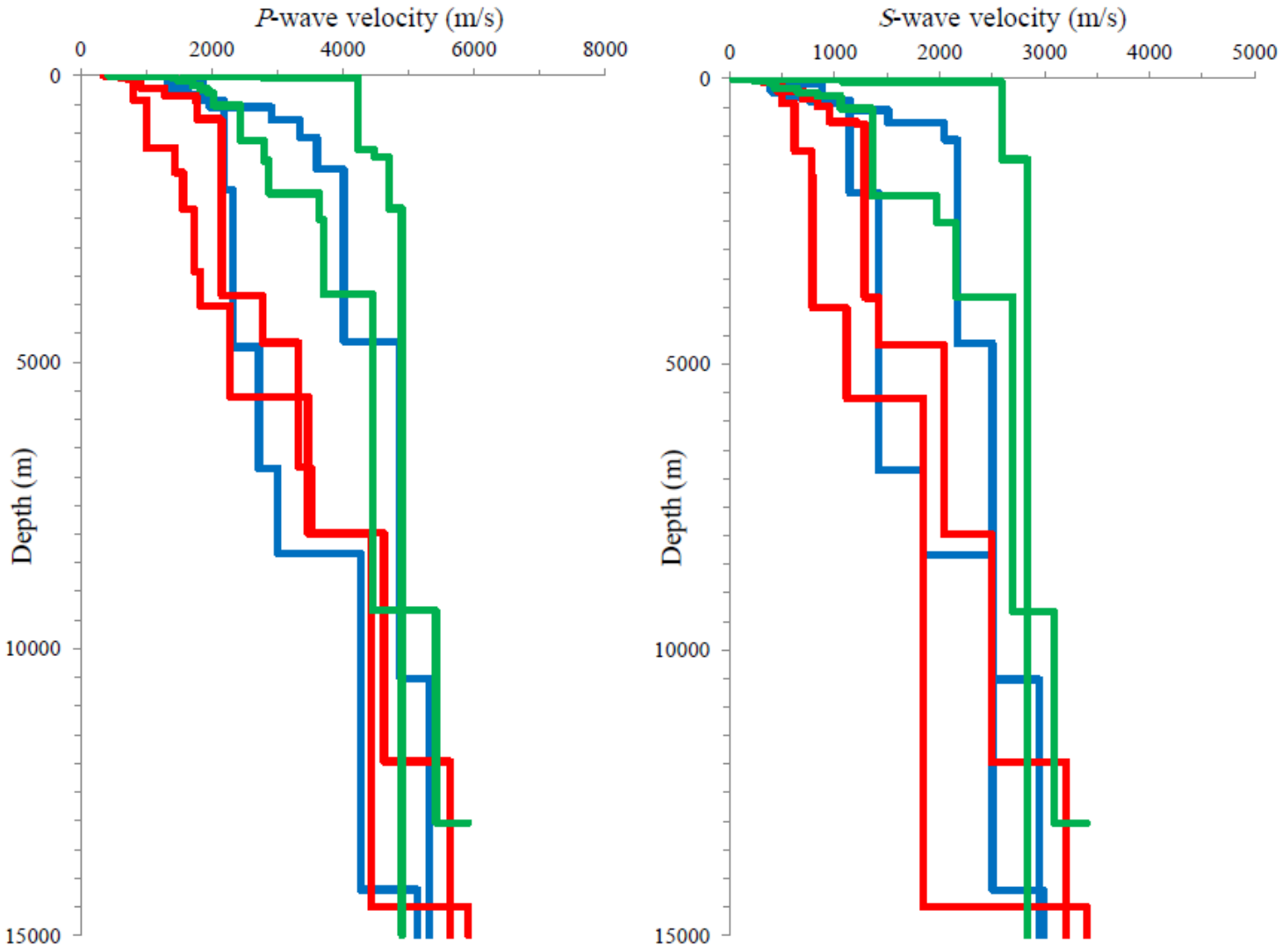

Figure 10

Inverted velocity structures in the East Hokkaido study area beneath stations on FW (blue), FZ (red), and HW (green).

Supplementary Files

This is a list of supplementary files associated with this preprint. Click to download.

- Suplementarymaterial.pdf